

Direct evidence of superdiffusive terahertz spin current arising from ultrafast demagnetization process

R. Gupta,^{1,2,*} F. Cosco,² R. S. Malik,² X. Chen,^{2,3} S. Saha,^{2,4} A. Ghosh,^{2,5} T. Pohlmann,⁶ J. R. L. Mardegan,⁶ S. Francoual,⁶ R. Stefanuik,² J. Söderström,² B. Sanyal,² O. Karis,² P. Svedlindh,¹ P. M. Oppeneer,² and R. Knut^{2,†}

¹*Department of Materials Science and Engineering,
Uppsala University, Box 35, SE-751 03, Uppsala, Sweden*

²*Department of Physics and Astronomy, Uppsala University, Box 516, SE-751 20, Uppsala, Sweden*

³*Department of Physics and Shenzhen Institute for Quantum Science & Engineering,
Southern University of Science and Technology, Shenzhen, Guangdong 518055, China*

⁴*Department of Physics, Ashoka University, 131029 Hariyana, India*

⁵*MAX IV Laboratory, Lund University, SE-22 100, Lund, Sweden*

⁶*Deutsches Elektronen-Synchrotron (DESY), Notkestrasse 85, D-22607 Hamburg, Germany*

(Dated: May 18, 2022)

Using element-specific measurements of the ultrafast demagnetization of Ru/Fe₆₅Co₃₅ heterostructures, we show that Ru can exhibit a significant magnetic contrast (5% asymmetry) resulting from ultrafast spin currents emanating from the demagnetization process of the FeCo layer. We use this magnetic contrast to investigate how superdiffusive spin currents are affected by the doping of heavy elements in the FeCo layer. We find that the spin currents are strongly suppressed by Re doping, in accordance with the theoretically predicted terahertz spin current in Ru, utilizing the superdiffusive spin transport model.

Since the discovery of ultrafast demagnetization by Beaupaire *et al.* [1] in 1996, showing that a ferromagnetic Ni film can be demagnetized on a subpicosecond time scale by fs laser pulse excitations, laser induced magnetization dynamics has received growing attention. The possibility to optically manipulate the magnetization on such fast time scales paves the way for terahertz (THz) operation of spintronic devices [2]. Moreover, ultrafast demagnetization of Ni results in THz emission being proportional to the second time-derivative of magnetization [3]. Besides technological relevance, research in this area has led to discoveries of novel phenomena like all-optical magnetization switching [4, 5], transfer of THz spin currents [6–8] and the optical inter-site spin transfer effect [9, 10].

For the last two decades, ultrafast magnetization dynamics of magnetic materials has been probed with femtosecond laser pulses using time-resolved techniques such as high harmonic generation (HHG) [11, 12], magnetic circular dichroism [13], and spin-polarized two-photon photoemission [14]. Several microscopic mechanisms have been proposed to explain the ultrafast dynamics including electron-photon mediated spin-flip scattering [15–17], electron-electron scattering [18], electron-magnon scattering [19], and direct transfer of angular momentum from photon to electron mediated by spin-orbit coupling [20, 21]. Malinowski *et al.* [22] first showed that laser-induced spin transport can enhance the demagnetization in metallic heterostructures. Superdiffusive spin transport [23] was proposed to play an important role in the laser-induced demagnetization process of

metallic magnetic films [6, 24–26]. However, other mechanisms to generate fast spin currents such as spin pumping were also proposed [27–29] and the origin of optically induced spin currents is being debated [30]. Spin-current injection through spin pumping [27, 29] should be favored by a stronger damping, but, although the latter can be engineered e.g. by doping of the ferromagnetic layer, such investigations are scarce.

Kampfrath *et al.* investigated the THz emission caused by the ultrafast laser-induced demagnetization of an Fe layer adjacent to nonmagnetic Ru and Au capping layers [7]. The measured temporal behavior of the THz spin currents was very different between the Ru and Au layers, which was explained by the different absorption of superdiffusive spin currents in the Ru and Au layers. In the case of Au, there are no empty *d*-states and the hot electrons injected into the *sp* states with high electron-band velocity will therefore be quickly reflected back into the magnetic layer. In the case of Ru, the *d*-band states with lower band velocities will transiently trap the injected spins and thus delay the spin current. However, as only the THz emission was measured, there was no *de facto* evidence of a superdiffusive spin current in the nonmagnetic layer.

The relation between ultrafast demagnetization and spin current generation is thus not yet understood and a direct evidence of superdiffusive THz spin currents via the demagnetization process is still elusive.

In this work, the combined effects of doping and choice of capping layer on the ultrafast magnetization dynamics are studied by using element-specific transverse magneto-optic Kerr effect (T-MOKE) and superdiffusive spin current simulations. Ru/Fe₆₅Co₃₅/Ru and Cu/Fe₆₅Co₃₅/Cu heterostructures are utilised as model systems, where rhenium (Re) is used as dopant in Fe₆₅Co₃₅ to modify the spin dynamics (cf. Fig. S1 in Sup-

* rahul.gupta@angstrom.uu.se

† ronny.knut@physics.uu.se

plemental Materials (SM)). The ultrafast spin dynamics is shown to be significantly different depending on choice of capping layer as well as on the doping concentration. A transient spin accumulation is evidenced in the Ru layer, which is absent for the Cu capped sample and this spin injection is significantly reduced with increasing Re doping concentration. Our simulations show that the THz spin current from the magnetic layer to the Ru layer is responsible for this increase in Kerr signal. However, electron scattering increases with increasing Re doping concentration, reducing the spin transport and therefore the transient spin accumulation in the Ru layer.

The Re doped (0, 3, 6, and 12.6 at.%) $\text{Fe}_{65}\text{Co}_{35}$ thin films were grown on SiO_2/Si substrate at room temperature using DC sputtering. Layers of Ru(3 nm) and Cu(5 nm) were used as seed and capping layers. The nominal thickness of $\text{Fe}_{65}\text{Co}_{35}$ was 20 nm, which was verified by x-ray reflectometry [31]. The distribution of the doping element within the films was characterized by Rutherford backscattering. The $\text{Fe}_{65}\text{Co}_{35}$ films exhibit a body-centered cubic structure, which was verified by x-ray diffraction using Cu $K_{\alpha 1}$ radiation. The lattice constant increases with increasing Re doping and follows the trend indicated by theoretical calculations. The deposition and characterization details can be found in Refs. [31–33].

The element-specific ultrafast magnetization dynamics of $\text{Fe}_{65}\text{Co}_{35}$ interfaced with Ru and Cu films as function of Re doping was studied using a table-top HHG setup [11, 34–36]. The table-top HHG setup uses the T-MOKE to measure the magnetic asymmetry of the signal. The laser is a chirped pulse amplification system running at a central wavelength of 800 nm with a maximum energy of 2 mJ per pulse and a pulse length of 35 fs. The laser beam is split into two parts; 80% of the laser beam is used for generating the XUV probe beam and 20% is used as a pump beam. The XUV probe beam is generated through a HHG process by focusing the laser light into a gas cell filled with helium [37, 38] that provides photons in the 32 – 72 eV energy range [34, 39, 40]. The incident angle between the sample and the probe beam is fixed at 45° in order to get maximum magnetic signal in the T-MOKE geometry [11, 41, 42]. The delay between pump and probe beams is controlled by a delay stage. An electromagnet with a magnetic field strength of ± 80 mT is used to magnetically saturate the sample. A detailed description of the experimental setup has been reported in Refs. [34, 35]. In the T-MOKE spectrometer, the sample is magnetized perpendicularly to the plane of incidence of the incoming p -polarized light [35]. The reflected light from the sample is recorded with a CCD camera. In order to obtain a magnetic contrast, the change in reflected intensity at the absorption edges of the different elements in the heterostructure was recorded for opposite directions of the magnetization. The resulting photon-energy dependent magnetic asymmetry $A(E)$ is the normalized difference of the reflected intensities for the two magne-

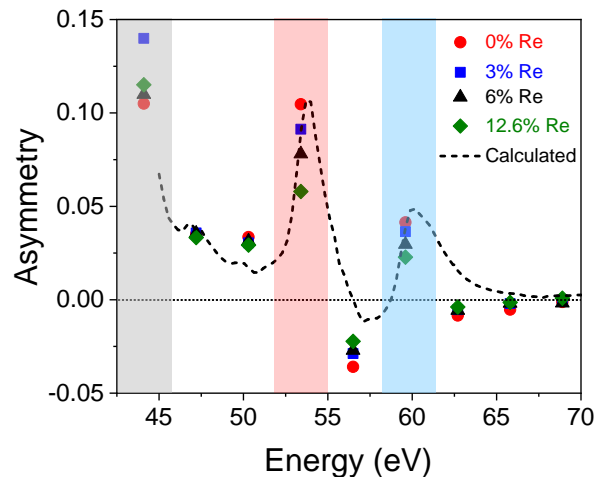


FIG. 1. Static T-MOKE asymmetries of Ru/ $\text{Fe}_{65}\text{Co}_{35}$ /Ru heterostructures with different Re doping. The different shaded regions represent the absorption edges of Ru (grey), Fe (red), and Co (blue). The black dotted line corresponds to the calculated asymmetry for the undoped sample.

tization directions [11, 43] and is defined as follows,

$$A(E) = \frac{[I_+(E) - I_-(E)]}{[I_+(E) + I_-(E)]}, \quad (1)$$

where $I_+(E)$ and $I_-(E)$ are the reflected intensities measured for the two different magnetization directions. This asymmetry is proportional to the magnetization of the sample as discussed in previous studies [11, 43–45].

Figure 1 shows the measured static Kerr asymmetry of Ru/ $\text{Fe}_{65}\text{Co}_{35}$ /Ru for different Re concentrations. The asymmetry is $\sim 10\%$ and $\sim 4\%$ at the $M_{2,3}$ -absorption edge of Fe (~ 54 eV) and Co (~ 60 eV), respectively. The asymmetry is reduced with increasing Re doping following the same trend as the saturation magnetization, which has already been reported [31, 33]. An additional large asymmetry is observed around 44 eV (grey region), which corresponds to the Ru $N_{2,3}$ -absorption edge. The magnitude of the Ru asymmetry is comparable to the Fe asymmetry at 54 eV. To verify that the asymmetry at 44 eV is related to Ru, a Cu/ $\text{Fe}_{65}\text{Co}_{35}$ /Cu heterostructure was studied for which no magnetic asymmetry near to 44 eV was observed (cf. Fig. S2 in SM).

Figure 1 shows the measured static Kerr asymmetry of Ru/ $\text{Fe}_{65}\text{Co}_{35}$ /Ru for different Re concentrations. The asymmetry is $\sim 10\%$ and $\sim 4\%$ at the $M_{2,3}$ -absorption edge of Fe (~ 54 eV) and Co (~ 60 eV), respectively. The asymmetry is reduced with increasing Re doping following the same trend as the saturation magnetization, which has already been reported [31, 33]. An additional large asymmetry is observed around 44 eV (grey region), which corresponds to the Ru $N_{2,3}$ -absorption edge. The magnitude of the Ru asymmetry is comparable to the Fe asymmetry at 54 eV. To verify that the asymmetry at 44 eV is related to Ru, a Cu/ $\text{Fe}_{65}\text{Co}_{35}$ /Cu heterostructure was studied for which no magnetic asymmetry near to 44 eV was observed (cf. Fig. S2 in SM).

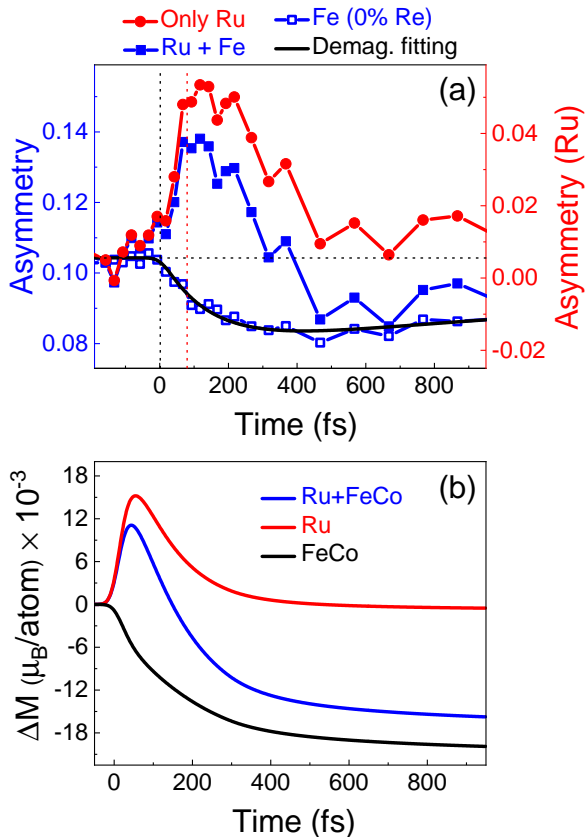


FIG. 2. (a) The time-dependent magnetic asymmetry measured at the Fe and Ru edges shown with blue solid and empty squares, respectively, for the undoped sample. The red circles correspond to the Ru asymmetry after subtracting the Fe contribution (black line). The left axis represents the scale for the blue squares (both solid and empty) whereas the right axis represents the scale for the Ru contribution alone. (b) Time-dependent magnetization in Ru and FeCo, computed with the superdiffusive transport model.

Using the formalism given by Zak *et al.* [46], we have calculated the magnetic asymmetry for the undoped heterostructure and presented it as a black dashed line in Fig 1. The magneto-optical (MO) parameters for Fe and Co were obtained from Willems *et al.* [9] and Valencia *et al.* [47]. The energy range of the simulated asymmetry is restricted to >45 eV by the available experimental energy range of the MO parameters. Both Ru and Cu are non-magnetic in these simulations. From these simulations it is clear that the weak MO component from Fe around 44 eV will result in a large asymmetry at the Ru $N_{2,3}$ absorption edge, while for the Cu capped sample the asymmetry at 44 eV remains low. It can, however, not be excluded that some of the asymmetry at the Ru absorption edge is due to an induced Ru magnetic moment coming from its proximity to the magnetic layer. Therefore, to further investigate the Ru magnetic asymmetry, we utilized element-specific synchrotron based x-ray techniques [48, 49]; x-ray absorption and magnetic reflectivity measurements carried out at the Ru L_3 ab-

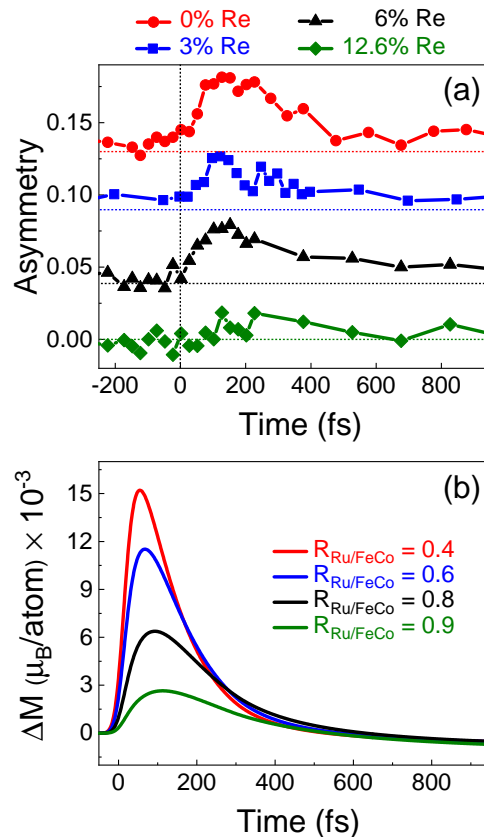


FIG. 3. (a) Ultrafast magnetization dynamics of Ru (after subtracting the Fe contribution) in $Fe_{65}Co_{35}$ films with different Re doping. An increase in the asymmetry signal is observed around time zero. The time-dependent change in asymmetry is strongest for the undoped sample and decreases with increasing Re doping. For better overview the ordinate for the asymmetry at the Ru edge is shifted for different Re doping. (b) Computed time-dependent magnetization in Ru for different reflection coefficients at the Ru/FeCo interface.

sorption edge reveal a magnetic asymmetry only present for the undoped sample, which is assigned to a magnetic proximity effect induced by the FeCo layers (cf. Sec. II in SM). This has also been verified by first-principles calculations based on density functional theory; it is observed that in the absence of Re doping, the induced magnetic moments in the Ru atomic layers close to the interface are larger than in the case of Re doped FeCo (cf. Sec. III in SM).

Figure 2(a) shows time- and element-resolved measurements for the Ru capped samples. The line with blue squares shows the Ru asymmetry during the demagnetization of the undoped sample. A large increase of the asymmetry ($\sim 5\%$) is observed after 100 fs, which has decreased to below the initial value after 500 fs. The initial rise of the asymmetry is attributed to spin currents that spin polarise Ru and the subsequent decreased asymmetry is related to the decreased asymmetry of Fe, which has a significant contribution at the Ru edge. The Fe contribution, represented by the empty blue squares and

the fitted black solid line, can easily be subtracted from the Ru asymmetry at 44 eV. Note that the Fe asymmetry has been normalized to the Ru value before time zero. The remaining asymmetry then corresponds to the pure spin polarization of Ru, shown as red filled circles. It is clear that the peak of the Ru spin polarization occurs before the maximum demagnetization of Fe, and that this spin polarization is short lived ($\lesssim 500$) fs.

To confirm the aforementioned speculation, we calculated the laser-induced demagnetization of FeCo and the superdiffusive spin current in the Ru layer using the superdiffusive spin transport model, in which the ultrafast demagnetization process is the source of the spin current [23], i.e., $\partial m/\partial t \propto -\partial J_s/\partial z$, where $m(z, E, t)$ is the magnetization density and $J_s(z, E, t)$ the spin-current density through the interface, both dependent on the energy E of the hot electrons and the z coordinate perpendicular to the layers. The details of the model can be found in Sec. IV, SM. Figure 2(b) displays the computed laser-induced transient magnetization of the Ru layer and the laser induced demagnetization of the ferromagnetic FeCo layer, assuming an $\text{Fe}_{0.5}\text{Co}_{0.5}$ composition and using *ab initio* computed hot electron velocities and spin lifetimes from Ref. [50]. The magnetization of the Ru layer, displayed as a red solid line, consists of two contributions to properly treat the interface, $\Delta M_{\text{Ru}}(3 \text{ nm})$ and a small fraction of the magnetization of the ferromagnetic layer, $\Delta M_{\text{FeCo}}(0.2 \text{ nm})$. This is done because in the superdiffusive model material properties change abruptly from one layer to the other without taking into account hybridization and other interface effects. Thus, we notice that the Ru layer reaches its maximum magnetization at $t \sim 60$ fs, where $t = 0$ is taken at the peak of the gaussian laser pulse. Furthermore, after this fast magnetization the layer is demagnetized on a longer time-scale. This behavior can be explained through two competing processes: spin flips due to scattering events within the layer and reflections at the Ru/FeCo interface, which temporarily trap the hot electrons within the Ru layer slowing down the spin current flowing back into the FeCo layer. On the other hand, the magnetization of the FeCo layer shows the standard monotonic dynamics. Furthermore, by combining $\Delta M_{\text{Ru}}(3 \text{ nm})$ and $\Delta M_{\text{FeCo}}(20 \text{ nm})$, displayed as solid blue line, we observe a similar behaviour to the one shown in Fig. 2(a) by the Ru asymmetry at 44 eV without subtracting the Fe contribution.

The ultrafast dynamics at the Ru absorption edge for different Re concentrations are shown in Fig. 3(a). In all measurements, the pump fluence was adjusted so that all samples show similar amount of demagnetization ($\sim 20\%$) at the Fe edge. For the undoped sample, the asymmetry at the Ru edge is about $\sim 5\%$ (red curve). For the samples with 3 at% and 6 at% Re doping, the asymmetry signal decreases to $\sim 3\%$. For the 12.6 at% Re doped sample, the asymmetry is very weak and close to the noise level (green diamonds). Note that all curves (except for 12.6 at% Re) have been shifted vertically and that the

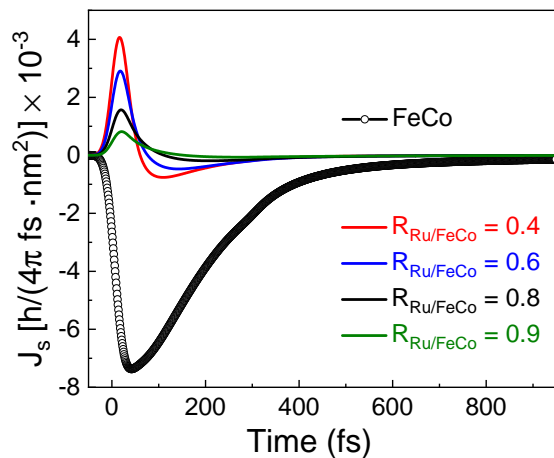


FIG. 4. Time-dependent spin current J_s in FeCo (black squares) and in Ru as a function of different reflection coefficients R , where $R=0.4$ corresponds to undoped FeCo.

horizontal dashed lines correspond to zero asymmetry.

Notably, Re doping attenuates the time dependent Ru asymmetry significantly, and for the 12.6 at.% Re doped sample the asymmetry is close to the detection limit. A reasonable explanation for this effect is that Re doping results in enhanced spin scattering, which effectively blocks the spin current from reaching the Ru layer as shown in Fig. S1(c), SM.

To mimic the effect of Re doping in the FeCo layer, we consider the hot electron dynamics in the presence of a higher reflection coefficient (R). The doping of the sample can be expected to increase the number of scattering events and thus reduce the effective transmission probability between the layers. Figure 3(b) shows the dynamics of the magnetization calculated for different values of the reflection coefficient, where $R = 0.4$ and 0.9 correspond to undoped FeCo and maximum doping of FeCo, respectively. We find that the magnitude of the magnetization decreases with an increase of reflection coefficient, which is in accordance with the experimentally observed magnetic asymmetry. Furthermore, higher reflection coefficients shift the maximum of the asymmetry to longer times. For the parameters considered, we observe a shift from $t \sim 60$ fs for $R = 0.4$ to $t \sim 100$ fs for $R = 0.9$, which is again in accordance with the experimental findings.

To further explore the laser-induced dynamics, we explicitly display the computed spin current in the layers as shown in Fig. 4. While the current in the FeCo layer never changes sign, the current in the Ru layer exhibits a sign change, signalling a relevant amount of electrons both entering and leaving the Ru layer.

The present measurements are consistent with superdiffusive spin-current injection into Ru, but other models based on spin injection through magnon spin pumping have also been proposed [27, 29, 30]. The latter models are expected to depend on the Gilbert damping parameter α , as larger damping implies stronger transfer of angular momentum and demagnetization. To cor-

roborate the relation between damping, demagnetization, and spin-current injection we have measured the demagnetization time τ_M and the damping parameter of the Re-doped films. Previously, it has been shown that the damping parameter of transition-metal films can be modified by introducing *4d*, *5d* or rare-earth dopants [32, 51–53]. Specifically, α increases more than four-fold for 12.6% Re doping in FeCo [31]. In models based on spin pumping through magnon damping [27, 29, 30] more Gilbert damping would imply an increasing loss of spin angular momentum and a spin voltage imbalance building up at the FeCo/Ru interface, leading to a larger spin current pumped into Ru. However, this behavior is not seen in our measurements. We note however that the relation between Gilbert damping and demagnetization time is not yet understood and can be material dependent. Koopmans *et al.* [15] derived an analytical expression that relates τ_M to α^{-1} . Walowski *et al.* [54] found contradicting results; α increased with rare-earth metal doping in permalloy while a constant τ_M was observed. Radu *et al.* [55] showed that the dynamics of rare-earth metal doped permalloy exhibits an increase of both the demagnetization and remagnetization time constants. Here, using Re doping, we also observe that τ_M is constant whereas α increases significantly (cf. Fig. S4(a), SM), providing direct evidence for a decreased spin current injection with Re doping, in agreement with our spin current calculations.

Lastly, the superdiffusive spin current in the Ru layer will act as an electric dipole source of electromagnetic radiation in the THz frequency band [7], a phenomenon that has received attention recently [56–59]. In Fig. S7 of the SM we show the Fourier transform of the superdiffusive spin current in the Ru layer. We find that, while the peak THz value is below ~ 2 THz, the THz emission amplitude is predicted to decay to 10% at a bandwidth of ~ 18 THz. Furthermore, we find that the amplitude and bandwidth of the spectrum decrease as the reflection coefficient increases, which is in accord with the amplitude of the spin current in the Ru layer decreasing with increasing reflection coefficient. This exemplifies that engineering the ferromagnet using Re doping offers possibilities to engineer the THz emission.

In conclusion, we have used an element-selective probe to show that a capping layer of Ru exhibits a large increase in magnetic asymmetry at the Ru $N_{2,3}$ -absorption edge caused by ultrafast demagnetization of the adjacent FeCo layer. It is notably necessary to use an element-selective probe, otherwise the signal from the magnetic layer will fully obscure any magnetic signal from the capping layer. The measured spin injection into the Ru layer and the demagnetization of the FeCo layer, as well as the

influence of Re doping, are well explained by superdiffusive THz spin currents. Apart from earlier measurements of ultrafast spin dynamics in interlayer exchange-coupled magnetic structures elucidating the effect of superdiffusive spin currents on the process of ultrafast spin dynamics [6], direct measurements as presented here of spin injection in nonmagnetic materials due to superdiffusive spin currents have not been reported before. We have utilized the Ru layer as a detector of spin polarized currents emanating from a doped $Fe_{65}Co_{35}$ layer upon ultrafast demagnetization. We have doped the $Fe_{65}Co_{35}$ layer with different concentrations of the *5d* element Re, which has been shown to have a significant effect on the Gilbert damping parameter [31]. We have shown that Re doping of $Fe_{65}Co_{35}$ decreases the amount of spin accumulation in the Ru layer. As explained by our spin current simulations, the amount of superdiffusive THz spin current entering the Ru layer decreases due to scattering at Re sites. The reduced spin current is predicted to yield a reduction of the amplitude of THz emission spectrum and bandwidth in the frequency domain. Our finding bears significance for the development of devices utilizing superdiffusive spin currents to generate broadband THz radiation as these could greatly benefit from the possibility to directly measure the amplitude of the spin current. Moreover, the direct evidence of a superdiffusive THz spin current in a nonmagnetic metal generated by ultrafast demagnetization opens a plethora of possibilities to further engineer magnetic heterostructures for high-speed spintronic devices.

This work is supported by the Swedish Research Council (VR, contract 2017-03799), the Olle Engkvists Stiftelse (Grant No. 182-0365) and by the Swedish National Infrastructure for Computing (SNIC), through grant agreement No. 2018-05973. This work is furthermore funded by the European Union’s Horizon2020 Research and Innovation Programme under FET-OPEN Grant agreement No. 863155 (s-Nebula). P.M.O. acknowledges support by the Deutsche Forschungsgemeinschaft through CRC/TRR 227 “Ultrafast Spin Dynamics”, project MF. R.G. acknowledges DESY (Hamburg, Germany), a member of the Helmholtz Association HGF, for the provision of experimental facilities. Parts of this research were carried out at beamline P09 at PETRA III under proposal I-20200894 EC. We would like to acknowledge and thank M.Sc. Dominik Graulich, Dr. Timo Kuschel (Bielefeld University) for developing within the long-term project LTP I-20170016 the vacuum chamber for the vector electromagnet used in this work and Prof. Günter Reiss (Bielefeld University) for contributing within LTP II-20190009 the in-vacuum silicon drift detector used in this work.

[1] E. Beaurepaire, J.-C. Merle, A. Daunois, and J.-Y. Bigot, *Phys. Rev. Lett.* **76**, 4250 (1996).

[2] W. Zhang, P. Maldonado, Z. Jin, T. S. Seifert, J. Arabski, G. Schmerber, E. Beaurepaire, M. Bonn, T. Kampfrath,

- P. M. Oppeneer, and D. Turchinovich, *Nature Communications* **11**, 4247 (2020).
- [3] E. Beaurepaire, G. Turner, S. Harrel, M. Beard, J.-Y. Bigot, and C. Schmuttenmaer, *Applied Physics Letters* **84**, 3465 (2004).
- [4] C. D. Stanciu, F. Hansteen, A. V. Kimel, A. Kirilyuk, A. Tsukamoto, A. Itoh, and T. Rasing, *Phys. Rev. Lett.* **99**, 047601 (2007).
- [5] J. Gorchon, C.-H. Lambert, Y. Yang, A. Pattabi, R. B. Wilson, S. Salahuddin, and J. Bokor, *Applied Physics Letters* **111**, 042401 (2017).
- [6] D. Rudolf, C. La-O-Vorakiat, M. Battiato, R. Adam, J. M. Shaw, E. Turgut, P. Maldonado, S. Mathias, P. Grychtol, H. T. Nembach, T. J. Silva, M. Aeschlimann, H. C. Kapteyn, M. M. Murnane, C. M. Schneider, and P. M. Oppeneer, *Nature Communications* **3**, 1037 (2012).
- [7] T. Kampfrath, M. Battiato, P. Maldonado, G. Eilers, J. Nötzold, S. Mährlein, V. Zbarsky, F. Freimuth, Y. Mokrousov, S. Blügel, M. Wolf, I. Radu, P. M. Oppeneer, and M. Münzenberg, *Nature Nanotechnology* **8**, 256 (2013).
- [8] A. J. Schellekens, K. C. Kuiper, R. de Wit, and B. Koopmans, *Nature Communications* **5**, 4333 (2014).
- [9] F. Willems, C. von Korff Schmising, C. Strüber, D. Schick, J. K. Engel, Dieter W. and Dewhurst, P. Elliott, S. Sharma, and S. Eisebitt, *Nature Communications* **11**, 871 (2020).
- [10] P. Tengdin, C. Gentry, A. Blonsky, D. Zusin, M. Gerrity, L. Hellbrück, M. Hofherr, J. Shaw, Y. Kvashnin, E. K. Delczeg-Czirjak, M. Arora, H. Nembach, T. J. Silva, S. Mathias, M. Aeschlimann, H. C. Kapteyn, D. Thonig, K. Koumpouras, O. Eriksson, and M. M. Murnane, *Science Advances* **6**, eaaz1100 (2020).
- [11] S. Mathias, C. La-O-Vorakiat, P. Grychtol, P. Granitzka, E. Turgut, J. M. Shaw, R. Adam, H. T. Nembach, M. E. Siemens, S. Eich, C. M. Schneider, T. J. Silva, M. Aeschlimann, M. M. Murnane, and H. C. Kapteyn, *Proc. Natl. Acad. Sci. USA* **109**, 4792 (2012).
- [12] E. Turgut, C. La-o vorakiat, J. M. Shaw, P. Grychtol, H. T. Nembach, D. Rudolf, R. Adam, M. Aeschlimann, C. M. Schneider, T. J. Silva, M. M. Murnane, H. C. Kapteyn, and S. Mathias, *Phys. Rev. Lett.* **110**, 197201 (2013).
- [13] C. Stamm, T. Kachel, N. Pontius, R. Mitzner, T. Quast, K. Holldack, S. Khan, C. Lupulescu, E. F. Aziz, M. Wietstruk, H. A. Dürr, and W. Eberhardt, *Nature Materials* **6**, 740 (2007).
- [14] A. B. Schmidt, M. Pickel, M. Donath, P. Buczek, A. Ernst, V. P. Zhukov, P. M. Echenique, L. M. Sandratskii, E. V. Chulkov, and M. Weinelt, *Phys. Rev. Lett.* **105**, 197401 (2010).
- [15] B. Koopmans, J. J. M. Ruigrok, F. D. Longa, and W. J. M. de Jonge, *Phys. Rev. Lett.* **95**, 267207 (2005).
- [16] B. Koopmans, G. Malinowski, F. Dalla Longa, D. Steiauf, M. Fähnle, T. Roth, M. Cinchetti, and M. Aeschlimann, *Nature Materials* **9**, 259 (2010).
- [17] D. Steiauf and M. Fähnle, *Phys. Rev. B* **79**, 140401 (2009).
- [18] M. Krauß, T. Roth, S. Alebrand, D. Steil, M. Cinchetti, M. Aeschlimann, and H. C. Schneider, *Phys. Rev. B* **80**, 180407 (2009).
- [19] E. Carpene, E. Mancini, C. Dallera, M. Brenna, E. Puppin, and S. De Silvestri, *Phys. Rev. B* **78**, 174422 (2008).
- [20] F. Dalla Longa, J. T. Kohlhepp, W. J. M. de Jonge, and B. Koopmans, *Phys. Rev. B* **75**, 224431 (2007).
- [21] G. P. Zhang and W. Hübner, *Phys. Rev. Lett.* **85**, 3025 (2000).
- [22] G. Malinowski, F. Dalla Longa, J. H. H. Rietjens, P. V. Paluskar, R. Huijink, H. J. M. Swagten, and B. Koopmans, *Nature Physics* **4**, 855 (2008).
- [23] M. Battiato, K. Carva, and P. M. Oppeneer, *Phys. Rev. Lett.* **105**, 027203 (2010).
- [24] A. Eschenlohr, M. Battiato, P. Maldonado, N. Pontius, T. Kachel, K. Holldack, R. Mitzner, A. Föhlich, P. M. Oppeneer, and C. Stamm, *Nature Materials* **12**, 332 (2013).
- [25] N. Berggaard, M. Hehn, S. Mangin, G. Lengaigne, F. Montaigne, M. L. M. Laliu, B. Koopmans, and G. Malinowski, *Phys. Rev. Lett.* **117**, 147203 (2016).
- [26] M. Hofherr, P. Maldonado, O. Schmitt, M. Berritta, U. Bierbrauer, S. Sadashivaiah, A. J. Schellekens, B. Koopmans, D. Steil, M. Cinchetti, B. Stadtmüller, P. M. Oppeneer, S. Mathias, and M. Aeschlimann, *Phys. Rev. B* **96**, 100403 (2017).
- [27] G.-M. Choi, C.-H. Moon, B.-C. Min, K.-J. Lee, and D. G. Cahill, *Nature Physics* **11**, 576 (2015).
- [28] Q. Remy, J. Igarashi, S. Iihama, G. Malinowski, M. Hehn, J. Gorchon, J. Hohlfeld, S. Fukami, H. Ohno, and S. Mangin, *Adv. Sci.* **7**, 2001996 (2020).
- [29] M. Beens, R. A. Duine, and B. Koopmans, *Phys. Rev. B* **102**, 054442 (2020).
- [30] T. Lichtenberg, M. Beens, M. H. Jansen, B. Koopmans, and R. A. Duine, *Phys. Rev. B* **105**, 144416 (2022).
- [31] R. Gupta, N. Behera, V. A. Venugopal, S. Basu, A. K. Puri, P. Ström, M. A. Gubbins, L. Bergqvist, R. Brucas, P. Svedlindh, and A. Kumar, *Phys. Rev. B* **101**, 024401 (2020).
- [32] S. Akansel, V. A. Venugopal, A. Kumar, R. Gupta, R. Brucas, S. George, A. Neagu, C.-W. Tai, M. Gubbins, G. Andersson, and P. Svedlindh, *Journal of Physics D: Applied Physics* **51**, 305001 (2018).
- [33] S. Akansel, A. Kumar, V. A. Venugopal, R. Esteban-Puyuelo, R. Banerjee, C. Autieri, R. Brucas, N. Behera, M. A. Sortica, D. Primetzhofer, S. Basu, M. A. Gubbins, B. Sanyal, and P. Svedlindh, *Phys. Rev. B* **99**, 174408 (2019).
- [34] S. Plogmaker, J. A. Terschlüsen, N. Krebs, M. Svanqvist, J. Forsberg, U. B. Cappel, J.-E. Rubensson, H. Siegbahn, and J. Söderström, *Rev. Sci. Instrum.* **86**, 123107 (2015).
- [35] S. Jana, J. A. Terschlüsen, R. Stefanuik, S. Plogmaker, S. Troisi, R. S. Malik, M. Svanqvist, R. Knut, J. Söderström, and O. Karis, *Rev. Sci. Instrum.* **88**, 033113 (2017).
- [36] R. Stefanuik, R. Knut, S. Jana, J. Terschlüsen, A. Sandell, and J. Söderström, *Journal of Electron Spectroscopy and Related Phenomena* **224**, 33 (2018).
- [37] P. B. Corkum, *Phys. Rev. Lett.* **71**, 1994 (1993).
- [38] M. Lewenstein, P. Balcou, M. Y. Ivanov, A. L'Huillier, and P. B. Corkum, *Phys. Rev. A* **49**, 2117 (1994).
- [39] H. C. Kapteyn, M. M. Murnane, and I. P. Christov, *Phys. Today* **58**, 39 (2005).
- [40] T. Popmintchev, M.-C. Chen, P. Arpin, M. M. Murnane, and H. C. Kapteyn, *Nature Photonics* **4**, 822 (2010).
- [41] M. Hecker, P. M. Oppeneer, S. Valencia, H.-C. Mertins, and C. M. Schneider, *J. Electron Spectrosc. Relat. Phenom.* **144**, 881 (2005).
- [42] P. M. Oppeneer, *Handbook of Magnetic Materials*, Vol.

- 13, edited by K. H. J. Buschow (Elsevier, Amsterdam, 2001).
- [43] S. Jana, R. S. Malik, Y. O. Kvashnin, I. L. M. Locht, R. Knut, R. Stefanuik, I. Di Marco, A. N. Yaresko, M. Ahlberg, J. Åkerman, R. Chimata, M. Battiato, J. Söderström, O. Eriksson, and O. Karis, *Phys. Rev. Research* **2**, 013180 (2020).
- [44] S. Mathias, C. La-O-Vorakiat, J. M. Shaw, E. Turgut, P. Grychtol, R. Adam, D. Rudolf, H. T. Nembach, T. J. Silva, M. Aeschlimann, C. M. Schneider, H. C. Kapteyn, and M. M. Murnane, *Journal of Electron Spectroscopy and Related Phenomena* **189**, 164 (2013).
- [45] C. La-O-Vorakiat, E. Turgut, C. A. Teale, H. C. Kapteyn, M. M. Murnane, S. Mathias, M. Aeschlimann, C. M. Schneider, J. M. Shaw, H. T. Nembach, and T. J. Silva, *Phys. Rev. X* **2**, 011005 (2012).
- [46] J. Zak, E. R. Moog, C. Liu, and S. D. Bader, *Phys. Rev. B* **43**, 6423 (1991).
- [47] S. Valencia, A. Gaupp, W. Gudat, H.-C. Mertins, P. M. Oppeneer, D. Abramssohn, and C. M. Schneider, *New Journal of Physics* **8**, 254 (2006).
- [48] C. Klewe, T. Kuschel, J.-M. Schmalhorst, F. Bertram, O. Kuschel, J. Wollschläger, J. Stremper, M. Meinert, and G. Reiss, *Phys. Rev. B* **93**, 214440 (2016).
- [49] A. Moskaltsova, J. Krieff, D. Graulich, T. Matalla-Wagner, and T. Kuschel, *AIP Advances* **10**, 015154 (2020).
- [50] I. A. Nechaev and E. V. Chulkov, *Phys. Solid State* **51**, 754 (2009).
- [51] J. O. Rantschler, R. D. McMichael, A. Castillo, A. J. Shapiro, W. F. Egelhoff, B. B. Maranville, D. Pugalurtha, A. P. Chen, and L. M. Connors, *Journal of Applied Physics* **101**, 033911 (2007).
- [52] G. Woltersdorf, M. Kiessling, G. Meyer, J.-U. Thiele, and C. H. Back, *Phys. Rev. Lett.* **102**, 257602 (2009).
- [53] A. Rebei and J. Hohlfeld, *Phys. Rev. Lett.* **97**, 117601 (2006).
- [54] J. Walowski, G. Müller, M. Djordjevic, M. Münzenberg, M. Kläui, C. A. F. Vaz, and J. A. C. Bland, *Phys. Rev. Lett.* **101**, 237401 (2008).
- [55] I. Radu, G. Woltersdorf, M. Kiessling, A. Melnikov, U. Bovensiepen, J.-U. Thiele, and C. H. Back, *Phys. Rev. Lett.* **102**, 117201 (2009).
- [56] D. M. Nenno, R. Binder, and H. C. Schneider, *Phys. Rev. Applied* **11**, 054083 (2019).
- [57] T. H. Dang, J. Hawecker, E. Rongione, G. Baez Flores, D. Q. To, J. C. Rojas-Sanchez, H. Nong, J. Mangeney, J. Tignon, F. Godel, S. Collin, P. Seneor, M. Bibes, A. Fert, M. Anane, J.-M. George, L. Vila, M. Cosset-Cheneau, D. Dolfi, R. Lebrun, P. Bortolotti, K. Belashchenko, S. Dhillon, and H. Jaffrès, *Applied Physics Reviews* **7**, 041409 (2020).
- [58] E. T. Papaioannou and R. Beigang, *Nanophotonics* **10**, 1243 (2021).
- [59] C. Bull, S. M. Hewett, R. Ji, C.-H. Lin, T. Thomson, D. M. Graham, and P. W. Nutter, *APL Materials* **9**, 090701 (2021).